Author/s:
Sun, H;Cleary, JO;Glarin, R;Kolbe, SC;Ordidge, RJ;Moffat, BA;Pike, GB

Title:
Extracting more for less: multi-echo MP2RAGE for simultaneous T1-weighted imaging, T1 mapping, $R2*$ mapping, SWI, and QSM from a single acquisition

Date:
2020-04-01

Citation:
Sun, H., Cleary, J. O., Glarin, R., Kolbe, S. C., Ordidge, R. J., Moffat, B. A. & Pike, G. B. (2020). Extracting more for less: multi-echo MP2RAGE for simultaneous T1-weighted imaging, T1 mapping, $R2*$ mapping, SWI, and QSM from a single acquisition. Magnetic Resonance in Medicine, 83 (4), pp.1178-1191. https://doi.org/10.1002/mrm.27975.

Persistent Link:
https://hdl.handle.net/11343/286399

DR. HONGFU SUN (Orcid ID : 0000-0003-3436-7831)

Article type : Full Paper

Extracting more for less: Multi-echo MP2RAGE for simultaneous T1-weighted imaging, T1 mapping, R2* mapping, SWI, and QSM from a single acquisition

Hongfu Sun[1,2*], Jon O. Cleary[3,4], Rebecca Glarin[3], Scott C. Kolbe[3,5], Roger J. Ordidge[3], Bradford A. Moffat[3], G. Bruce Pike[2]

[1]School of Information Technology and Electrical Engineering, University of Queensland, Brisbane, Queensland 4072 Australia

[2]Department of Radiology, University of Calgary, 3330 Hospital Dr. NW, Calgary, Alberta T2N 1N4 Canada

[3]Department of Medicine and Radiology, University of Melbourne, Parkville, Victoria 3052 Australia

[4]Department of Radiology, Guy's and St. Thomas' NHS Foundation Trust, London, U.K.

[5]Department of Neuroscience, Monash University, Melbourne, Victoria 3004 Australia

*Correspondence to: Hongfu Sun, School of Information Technology and Electrical Engineering, General Purpose South (Building 78), University of Queensland, St Lucia campus, Queensland 4072 Australia. Phone: +61 7 336 54307. Email: hongfu.sun@uq.edu.au

Word count: 4861 words

This is the author manuscript accepted for publication and has undergone full peer review but has not been through the copyediting, typesetting, pagination and proofreading process, which may lead to differences between this version and the Version of Record. Please cite this article as doi: 10.1002/MRM.27975

ABSTRACT

Purpose: To demonstrate simultaneous T1-weighted imaging, T1 mapping, R2* mapping, SWI, and QSM from a single multi-echo (ME-) MP2RAGE acquisition.

Methods: A single-echo (SE-) MP2RAGE sequence at 7 T was extended to multi-echo with 4 bipolar GRE readouts. T1-weighted images and T1 maps calculated from individual echoes were combined using sum-of-squares and averaged, respectively. Multi-echo combined SWI and associated minimum intensity projection (mIP) images were generated with echo-time adjusted homodyne filters. A QSM reconstruction pipeline was used, including a novel Phase-Offsets Estimation from Multi-echoes (POEM) method to properly combine the phase images from the 32 receiver channels. Measurements of susceptibility, R2* and T1 of brain tissue from ME-MP2RAGE were compared with those from standard multi-echo (ME-) GRE and SE-MP2RAGE.

Results: The multi-echo combined T1-weighted, T1 map, SWI, and mIP images showed increased SNRs compared to the single-echo results. The proposed POEM coil combination method led to QSM results free of phase-singularity artifacts, which were present in the standard adaptive combination method. T1-weighted, T1 and susceptibility maps from ME-MP2RAGE were comparable to those obtained from SE-MP2RAGE and ME-GRE, while R2* maps showed increased blurring and reduced SNR. T1, R2* and susceptibility values of brain tissue from ME-MP2RAGE were consistent with those from SE-MP2RAGE and ME-GRE.

Conclusion: High resolution structural T1 weighted imaging, T1 mapping, R2* mapping, SWI, and QSM can be extracted from a single 8.5-minute ME-MP2RAGE acquisition using a customized reconstruction pipeline. This method can be applied to replace separate SE-MP2RAGE and ME-GRE acquisitions to significantly shorten total scan time.

KEYWORDS: ME-MP2RAGE, QSM, POEM, multi-parametric mapping, coil combination, magnetic susceptibility

INTRODUCTION

Clinical and research brain MRI protocols typically include multiple acquisitions using different pulse sequences to obtain various image contrasts and to quantitatively map tissue properties, with each additional acquisition increasing scan time. A single MRI acquisition, of clinically acceptable scan time, that can produce multiple image contrasts and quantitative maps is beneficial for time efficiency and inherent image registration. A high-quality T1-weighted anatomical scan, providing excellent image contrast between grey matter (GM), white matter (WM), and cerebrospinal fluid (CSF), has become an essential part of clinical and research protocols for structural visualization, image segmentation, registration, and morphometry. The MPRAGE sequence[1] has been widely adopted at clinical field strengths (i.e. 1.5 T and 3 T) for T1-weighted imaging. To mitigate the increased B_1 field inhomogeneity effects that degrade the MPRAGE image quality at ultra-high field (e.g. 7 T), an MP2RAGE (Magnetization Prepared 2 Rapid Acquisition Gradient Echoes) sequence that combines signals acquired at two different effective inversion times has been proposed.[2] The MP2RAGE sequence also enables T1 mapping, which quantifies the longitudinal relaxation time of tissue, without the confounds of proton density, T2*, and receiver B_1 field inhomogeneity effects.[2]

A recent extension of the single-echo MP2RAGE (SE-MP2RAGE) to multi-echo (ME-MP2RAGE) substantially broadened the multi-parametric imaging capability of the sequence.[3–5] Relatively longer echo times in the latter echoes of the ME-MP2RAGE readouts enable susceptibility-induced image contrasts, such as T2*-weighted, GRE phase,[6,7] and SWI,[8] as well as quantitative techniques, such as R2* mapping and QSM.[9–14] These methods have been used to study brain iron changes in healthy aging[15–17] and various neurological diseases,[18,19] micro-bleeding or hemorrhage in stroke populations,[20–24] as well as myelin changes in multiple sclerosis lesions and normal appearing white matter.[25,26] In particular, QSM has recently been the source of significant methodological development due to its potential for clinical applications and neuroscience research. QSM involves a deconvolution of GRE phase maps to recover local susceptibility sources, which solves non-local and orientation dependency problems that are characteristic of conventional phase imaging and SWI. Also, QSM enables quantitative measurements of the tissue susceptibility property that is independent of field strength and sequence parameters. However, QSM reconstruction is non-trivial and involves several critical pre-processing steps, including the combination of multi-channel phase images. Coil

combination of phase images becomes more challenging at ultra-high field due to the lack of information from a uniform body coil. Recently, coil combination methods have been proposed that do not require a uniform body coil. One method uses an ultra-short TE reference scan,[27] which adds scan time and requires image registration. Another approach requires multi-echoes with specific TEs,[28] which limits the sequence parameters. The default adaptive coil combination method for GRE phase imaging used on ultra-high field Siemens scanners is sub-optimal and often leads to phase singularities and poor SNR in the combined phase images. Using such degraded phase images as input to the QSM reconstruction pipeline can result in severe artifacts in the final QSM images. This has been reported in the original ME-MP2RAGE implementation at 7 T,[3] where QSM images suffered from substantial artifacts that significantly limit their value. The other limitation of the ME-MP2RAGE technique from Metere et al.'s is the long scan duration (~20 min). In Metere et al.'s implementation, GRAPPA was implemented in the second phase-encoding direction (i.e. inside the inversion loop) to fit in more echoes with longer TEs. Another recent implementation at 7 T proposed by Caan et al.[5] acquired single echo only in the first inversion block, while extending the GRE readouts during the second inversion block to multiple echoes (last echo time 28.5 ms). This method makes the first inversion time more flexible, which can be chosen to optimize the T1-weighted contrast, and also slightly shortened scan duration (16:30 min). Multi-echo MP2RAGE has also been studied at 3 T by Jutras et al.[4] with the last echo time of 13.8 ms. In that study, QSM was not computed, however, R2* map displayed low SNR due to the short echo times at 3 T.

In this study, we substantially reduce the 7 T ME-MP2RAGE sequence duration, by implementing GRAPPA in the first phase-encoding direction (i.e. outside the inversion loop) and keeping the TEs relatively short and efficient with bipolar readouts, to achieve a clinically acceptable scan time (8:27 min) for high resolution whole brain imaging, and produce anatomical T1-weighted images, T1 maps, SWI, minimum intensity projection (mIP) images, R2* maps and QSM, simultaneously. The effect of multi-echo combination on the T1-weighted images, T1 maps, and SWI is investigated. We introduce a novel phase-offset correction and coil combination method that produces combined phase images with no singularities and demonstrate its impact on the final QSM quality, using bipolar readouts. Different tissue properties of basal ganglia, white matter, and cortical grey matter, including T1, susceptibility, and R2*, measured

from the ME-MP2RAGE sequence are compared with the literature and also with those obtained from standard SE-MP2RAGE and multi-echo GRE (ME-GRE) sequences.

METHODS

Pulse sequences and acquisition parameters

A standard MP2RAGE acquisition was extended to multi-echo (ME-MP2RAGE) using a prototype sequence on a 7 T whole-body research scanner (Siemens Healthcare, Erlangen, Germany). Different from the previous implementation[3] with GRAPPA inside the inversion loop and monopolar longer echo times, we used GRAPPA outside the inversion loop and bipolar shorter echo times to achieve a dramatically reduced total scan time. The modified sequence diagram is illustrated in Figure 1. A FOCI adiabatic inversion pulse was applied at the beginning of the sequence for magnetization preparation. Within each of the two inversion blocks, repeated excitations (α_1 and α_2) and readouts are performed while looping through the second phase-encoding dimension (kz); TI_1 and TI_2 correspond to the time between the center of the inversion pulse and the central lines of kz phase-encoding. A recovery time was appended at the end of the second GRE block before the next inversion pulse with a different gradient step in the first phase-encoding dimension (ky). Sequence parameters were: 3D whole head coverage using a FOV = 240×240×147 mm^3, voxel size = 0.75 mm isotropic, 4 bipolar readouts with TEs = 2.38/4.62/6.86/9.10 ms, GRE TR = 11.3 ms, TIs = 700/2700 ms, number of excitations per readout = 147, sequence TR = 5000 ms, BW = 540 Hz/Px, α_1/α_2= 8°/10°, GRAPPA acceleration factor of 3, 3/4 partial Fourier in both phase and slice directions, no flow compensation, and scan time = 8:27 mins.

A conventional high resolution ME-GRE acquisition, which is considered the standard for QSM and R2* mapping, was also performed for comparison. The ME-GRE acquisition parameters were: 3D whole head coverage using a FOV = 210×210×144 mm^3, voxel size = 0.75 mm isotropic, 9 bipolar readouts with first TE = 5.10 ms, echo spacing = 2.04 ms, last TE = 21.42 ms, TR = 24 ms, BW = 600 Hz/Px, α = 13°, GRAPPA acceleration factor of 2, full flow compensation of the first echo, and scan time = 9:25 mins. The conventional single-echo MP2RAGE was also performed to compare results of T1-weighted images and T1 maps with those from ME-MP2RAGE. The SE-MP2RAGE acquisition parameters were: 3D whole head

coverage using a FOV = 240x240x147 mm^3, voxel size = 0.75 mm isotropic, TE = 2.96 ms, GRE TR = 6.9 ms, TIs = 700/2700 ms, number of excitations per readout = 147, sequence TR = 5000 ms, BW = 240 Hz/Px, α_1/α_2 = 4°/5°, GRAPPA acceleration factor of 3, 3/4 partial Fourier in both phase and slice directions, no flow compensation, and scan time = 8:12 mins. For all acquisitions, a 32-channel head coil was used for signal reception. Nine healthy subjects (age: 34.4 ± 10.1, 3 females) were scanned using all three sequences (summarized in Table 1).

Echo-combination of T1-weighted image and quantitative T1 map

T1-weighted images and T1 maps were derived by combining the GRE signals at the two inversion times, according to the original MP2RAGE paper[2], for each echo time. Sum-of-squares and averaging methods were used to combine the T1-weighted images and T1 maps from individual echoes, respectively.

The echo-combined T1-weighted images and T1 maps were compared with results from individual echoes, and also compared with results from the standard single-echo MP2RAGE acquisition. A T1 difference map, between TE_1 and TE_4, as well as the standard deviation map for T1 values from all 4 TEs, were also computed.

Reconstruction and comparison of R2* maps

For the ME-MP2RAGE sequence, R2* was computed by mono-exponential fitting the magnitude images, from the second inversion time, as described previously.[29] R2* was also derived from the ME-GRE sequence using the same algorithm. To compare R2* maps from the two different sequences, the first-echo magnitude image at the second inversion time from the ME-MP2RAGE sequence and the first echo of the ME-GRE sequence were co-registered to a middle template image using FreeSurfer.[30] The transformation matrices were then applied to co-register the R2* maps from ME-MP2RAGE and ME-GRE. To investigate the effect of different ranges of TEs on R2* mapping, R2* fitting was also performed using a subset of the first three echoes (5.1, 7.14, 9.18 ms) from the ME-GRE sequence, which approximately matches the TE range covered in the ME-MP2RAGE sequence.

Multi-channel coil combination for phase imaging

The measured phase from individual receiver channels (φ_I) has three main components: one from the induced magnetic field (ΔB_0) that accumulates with echo time, one from the channel-dependent initial receiver phase-offset ($\varphi_{off,I}$), and one from eddy currents ($\varphi_{edd,p}$) originating from the readout gradients, which is dependent on the readout polarity (positive or negative):[31]

$$\varphi_I = -2\pi\gamma\Delta B_0 TE + \varphi_{off,I} + \varphi_{edd,p}.$$

The coil combination for phase becomes non-trivial due to different $\varphi_{off,I}$ in each receiver channel. The adaptive coil combination method[32] was used by default in the Siemens 7 T scanner output. However, open-ended fringe lines can occur in the adaptive combined phase images leading to severe artifacts in the processed phase and QSM images, especially if path-based phase unwrapping algorithms are used in the reconstruction pipeline.

Recently, we have introduced a method to estimate and remove the coil-channel and gradient polarity dependent phase-offsets before coil combination.[33,34] In this paper, we refer to the method as POEM (Phase-Offset Estimation from Multi-echo). The POEM method is conceptually similar to the dual-echo approach proposed by Robinson et al.[35] That method involved phase unwrapping of individual channels from two echo times, requiring 64 phase unwraps for 32 channel reception. However, individual-channel phase images usually have low SNR that can produce phase singularities in some regions. In contrast, the proposed POEM method requires only one phase unwrapping on the channel-combined echo-difference map. This significantly reduces the reconstruction time compared to the previous dual-echo approach, and importantly, significantly enhances the robustness of the method because the channel-combined echo-difference map has high SNR and usually short echo spacing, and thus is straightforward to unwrap.

With the POEM method, both the receiver $\varphi_{off,I}$ and eddy current phase-offsets $\varphi_{edd,p}$ from positive or negative polarity can be removed from each channel using the first two consecutive echoes of the same polarity:

$$\Delta\hat{\varphi}_I = \angle^{S_{2,I}/S_{1,I}} = -2\pi\gamma\Delta B_0\Delta TE.$$

The phase difference maps $\Delta\hat{\varphi}_I$ from all channels are combined (complex summation) and unwrapped (best-path method[36]), producing a phase map $\Delta\hat{\varphi}$ with effective echo time of ΔTE, free of receiver and eddy current phase-offsets. The theoretical phase, without phase-offsets, at TE_1 is then estimated as: $\hat{\varphi}_{TE_1} = \Delta\hat{\varphi} \cdot TE_1/\Delta TE = -2\pi\gamma\Delta B_0 TE_1$. The phase-offset (i.e. eddy

current and channel offset effects included) for an individual channel I is computed in the complex domain by subtracting the estimated $\hat{\varphi}_{TE_1}$ from the individual-channel phase measured at TE_1 ($\varphi_{TE_1,I}$):

$$\varphi_{off,I} + \varphi_{edd,p} = \varphi_{TE_1,I} - \hat{\varphi}_{TE_1}.$$

For the current dataset, real and imaginary parts of the phase-offsets were smoothed using a Gaussian filter with a sigma of 4 mm to remove any residual structural contrasts. For the bipolar sequence data (ME-MP2RAGE and ME-GRE), odd (positive) and even (negative) phase-offsets were estimated respectively due to different eddy current induced phase-offsets from different readout polarities. The POEM estimated phase-offsets were then removed from the raw phase and the offset-corrected phase images from multiple channels were combined by averaging in the complex domain.

Echo-combination of SWI and mIP

SWI is usually generated from a single-echo GRE acquisition, with raw phase homodyne-filtered and thresholded as a mask. The mask is multiplied several times (e.g. power of 4) before being multiplied by the magnitude image, as described in the original SWI paper.[8] Multi-echo SWI has been proposed[37] by applying variable filter widths (FWs) to the phase images of different echo times to generate multiple SWI images, and then averaging to produce a combined SWI. Using a similar strategy, for the ME-MP2RAGE sequence, phase images from the 4 echoes at the second inversion time were homodyne-filtered with FWs from 10% to 25% (with 5% increments) of k-space. The filtered phases were averaged and used to generate the phase mask. The fourth power of the phase mask was applied to the sum-of-squares combined magnitude image to produce an echo-combined SWI map. Minimum intensity projection (mIP) was performed on the averaged phase map over 15 mm of axial mid-brain slices for visualization of veins. To compare with conventional single-echo results, a similar process was also performed on the last echo (homodyne FW of 25%) of the ME-MP2RAGE to produce a single-echo SWI and mIP over the same brain coverage. SWI images from the ME-GRE sequence were also produced as described above, with phase images from the 9 echoes homodyne-filtered with FWs from 10% to 50% of k-space.

Reconstruction pipeline for QSM

Channel-combined phase images at the second inversion time, were unwrapped in 3D using a best-path method.[36] Note that phase images at the first inversion time were not usable due to the π phase shift between regions below and above the zero crossing of the inversion recovery curve (Figure 2). The unwrapped phase images were further corrected for any global 2π jumps between echoes.[38] The assumption is that the echo difference map between any two neighboring echoes $\Delta\varphi_{n-m}$ should be close to that between the first and second echo $\Delta\varphi_{2-1}$. An induced magnetic total field map ΔB was obtained by linearly fitting the echoes according to the equation: $\varphi = -\gamma \cdot \Delta B \cdot TE$, using least-squares minimization weighted by the magnitude of each echo. The total field map was normalized by the main field (i.e. 7 T) and expressed in units of parts-per-million (ppm). Binary brain tissue masks were generated using the brain extraction tool (BET)[39] from FSL by setting the fractional intensity threshold to 0.3 ("bet2 -f 0.3") and smoothness factor to 2 ("bet2 -w 2"), on the first-echo magnitude image at the second inversion time. Background field was removed using the RESHARP method[40] with a spherical kernel radius of 2 mm and a Tikhonov regularization parameter of 10^{-4}. Dipole field inversion for QSM was performed using the iLSQR method.[41]

MRI measurements of brain tissue

The magnitude images (first echo) from the three sequences (i.e. ME-MP2RAGE, SE-MP2RAGE, and ME-GRE) were co-registered to a middle template image using FreeSurfer.[42] After applying the transformation, the co-registered T1-weighted images from ME-MP2RAGE were registered to the Montreal Neurological Institute (MNI) template using Advanced Normalization Tools (ANTs) software.[43] The derived affine and non-linear deformation operations were concatenated and then applied to the T1 maps, R2* maps, and QSM of the same subject from all sequences, to map them into the MNI template.

Iron-rich basal ganglia structure labels in the ATAG young atlas[44] including globus pallidus (GP), putamen (PU), caudate (CN), red nucleus (RN) and substantia nigra (SN), as well as cerebral cortex and cerebral white matter labels from Harvard-Oxford atlas, were used as ROI masks, and mean susceptibility, R2*, and T1 values were calculated in each individual's native space after inverse transformation. These measurements were compared between different sequences using paired t-tests, including comparisons of R2* and QSM from ME-MP2RAGE to those from ME-GRE, as well as T1 map from ME-MP2RAGE to that from SE-MP2RAGE.

RESULTS

Multi-parametric outputs from ME-MP2RAGE

The raw and composite images of different contrasts from the ME-MP2RAGE sequence are illustrated in Figure 2. The T1-weighted image and T1 map both show excellent contrast between cortical GM, WM, CSF, and some basal ganglia structures, such as caudate and putamen. R2*, SWI, and especially QSM, show clear boundaries of globus pallidus and thalamus, in addition to caudate and putamen, which are difficult to delineate in T1 images. In addition, the mIP image illustrates excellent visualization of the veins.

T1-weighted image and quantitative T1 map

The T1-weighted images of 4 individual echoes as well as the sum-of-squares combined image are shown in Figure 3a. The cortical-GM/WM/CSF contrasts from different echoes appear very similar, however the SNR decreases with longer echo times, which is more evident in the zoomed-in images in the bottom row of Figure 3a. The sum-of-squares (SoS) combined T1-weighted volume maintains similar cortical-GM/WM/CSF image contrast while enhancing SNR. However, with the increase of TE in later echoes, more noticeable T2*-weighed contrast is induced in iron-rich basal ganglia structures. As shown in Supporting Information Figure S1, in the T1-weighted images from conventional SE-MP2RAGE (TE = 2.96 ms) and from the first echo of ME-MP2RAGE (TE = 2.38 ms), globus pallidus has little contrast to surrounding white matter (red arrow). However, in the weighted images from the last echo of ME-MP2RAGE (TE = 9.1 ms) and the SoS combined, globus pallidus appears much darker than surrounding white matter, due to more pronounced T2* contrast.

The quantitative T1 maps from multiple echoes and their average map are shown in Figure 3b. In general, the T1 maps display very similar contrast among different echoes. However, it is observed in the zoomed images at the bottom row of Figure 3b that SNR decreases with echo time. The average T1 map shows similar image contrast but with increased SNR. The comparison of T1 maps between the conventional SE-MP2RAGE and the echo-averaged ME-MP2RAGE is shown in Figure 4. T1 maps from the two MP2RAGE sequences appear very similar.

A voxel wise comparison of the quantitative T1 maps from multiple echoes is shown in Supporting Information Figure S2. Most of the differences between T1 maps from TE_1 and TE_4 occur near the frontal brain region due to the significant signal decay in longer echo time, as indicated by the red arrows. Standard deviation (std) maps show small values in a uniform white matter region, for example only 53 ms in the white ellipsoid ROI with a mean T1 value of ~1200 ms. The largest deviation is found in region near the sinus cavity, with a standard deviation of 257 ms in the black ellipsoid ROI with a T1 value of ~1600 ms. Note that there are larger standard deviations near borders of CSF regions, which is due to the partial volume effect in voxels with a mix of CSF and WM/GM.

Comparison of R2* maps from different sequences

R2* maps calculated from the 4 bipolar echoes at the second inversion time of the ME-MP2RAGE sequence were registered and compared to those calculated from the 9 bipolar echoes of the ME-GRE sequence in Figure 5. Iron-rich basal ganglia in three orthogonal slices show similar hyperintense contrast in both methods. However, there is a larger fitting residual, i.e. normalized sum-of-squared errors of prediction (SSE), in the ME-MP2RAGE than the ME-GRE sequence. Visually, R2* map from ME-MP2RAGE also appears noisier than from ME-GRE. While the SNR is difficult to accurately evaluate in the highly heterogenous human brain, a regional standard deviation was measured to give a sense of SNR for the sake of comparison, by drawing an ROI in white matter in the sagittal plane (white box), where R2* appears relatively uniform on both sequences. The standard deviation of ME-GRE is 2.6 s^{-1}, while the standard deviation of the ME-MP2RAGE is 4.0 s^{-1}, and the mean R2* value for both sequences is ~30 s^{-1}. In addition, the R2* map from ME-GRE appears sharper than that from ME-MP2RAGE due to the blurring effect of T1 inversion recovery in ME-MP2RAGE.

R2* maps of segmented GM and WM from three methods (i.e. 9-echo GRE, 3-echo GRE, and 4-echo ME-MP2RAGE) were compared in Supporting Information Figure S3. It can be seen that for GM all three methods look very similar, except in the cerebellum. However, for WM it is obvious that the two shorter echo trains look similar to each other and produce higher R2* estimates than longer TE 9-echo GRE sequence.

SWI and mIP from multiple echoes

Echo-combined SWI and mIP images of ME-MP2RAGE are compared with results from the single last echo of ME-MP2RAGE in Figure 6. It is observed that the echo-combined SWI shows better GM-WM contrast and significantly improves SNR compared to the single-echo SWI, as clearly shown in the zoomed-in images. The echo-combined mIP also displays more and higher contrast vessel projections than mIP from the last echo only.

SWI images from ME-MP2RAGE are compared with those from ME-GRE in Supporting Information Figure S4. It can be seen that SWI extracted from both sequences displayed enhanced contrast in iron-rich deep grey matter regions and veins. However, they have different GM-WM-CSF contrast due to their different weighted magnitude base. The magnitude of ME-MP2RAGE has more T1 mixed contrast than the ME-GRE. CSF appears much darker in ME-MP2RAGE than in ME-GRE, which makes it difficult to be distinguishable from veins.

POEM coil combination for phase

Siemens 7 T scanner default adaptive combined phase and the resulting local field and QSM are compared with results derived from the POEM combined phase in Figure 7. Arrows point to phase singularities (i.e. open-ended fringe lines) due to the phase combination error in the default adaptive-combine method. These phase singularity errors cause substantial artifacts in local field map and the final QSM image as shown in Figure 7a (arrows). Using the proposed POEM method, individual-channel phase-offsets in odd and even echoes are estimated and removed. The POEM combined phase images are free of singularities and lead to artifact-free local field maps and QSM, as illustrated in Figure 7b. The phase-offset difference, due to eddy currents, between odd and even echoes from different readout polarities is shown in Supporting Information Figure S5. The POEM method was also used to combine phase images for the multi-echo GRE sequence (i.e. 9 bipolar readouts) and the results are shown in Supporting Information Figure S6, where offset-corrected phase images from individual channels display similar phase wrap patterns. Multi-channel phase images are properly combined with no singularities and successful local field and QSM results are obtained following standard QSM reconstruction pipeline.

Comparison of QSM from different sequences

QSM images extracted from the ME-MP2RAGE sequence are co-registered to and compared with those from the ME-GRE sequence in three orthogonal slices in Figure 8. QSM images from the two sequences appear very similar. Iron-rich basal ganglia show hyperintense contrast while WM shows hypointense contrast in QSM from both ME-MP2RAGE and ME-GRE.

ROI measurements of brain tissue

T1, R2*, and susceptibilities measured in globus pallidus (GP), substantial nigra (SN), red nucleus (RN), putamen (PU), caudate nucleus (CN), cerebral WM, and cortical GM, from all 9 subjects are compared in the bar plots in Figure 9. In general, susceptibility and R2* decrease while T1 increase in the order of GP, SN, RN, PU, and CN. T1 values from ME-MP2RAGE are consistent with those from SE-MP2RAGE, while R2* and QSM measurements of basal ganglia, WM, and cortical GM from ME-MP2RAGE are consistent with those from ME-GRE. Paired t-tests found statistically significant differences (uncorrected, $P < 0.05$) in T1 values from ME-MP2RAGE and SE-MP2RAGE in SN (3.0%); R2* values from ME-MP2RAGE and ME-GRE in CN (10.0%) and WM (6.8%); susceptibility values from ME-MP2RAGE and ME-GRE in GP (5.3%). The measurements (i.e. susceptibility of 0.06 – 0.14 ppm; R2* of 40 – 80 s^{-1}; T1 of 1200 – 2000 ms) are consistent with literature.[45–47]

DISCUSSION

We have demonstrated a multi-echo MP2RAGE sequence at 7 T with tuned acquisition parameters to achieve whole brain multi-parametric imaging with sub-millimeter spatial resolution in about 8 and a half minutes. Using a customized image reconstruction pipeline, anatomical T1-weighted, T1 map, R2* map, SWI, mIP, and QSM images were derived from the single acquisition, which normally requires separate SE-MP2RAGE and ME-GRE acquisitions. The scan time of our ME-MP2RAGE is more than 50% shorter than the combined dual acquisitions. In addition to reducing scan time, the simultaneously acquired maps are intrinsically aligned, which eliminates the need for multi-modal image registrations that can be problematic, especially at ultra-high fields. Furthermore, the combination of different contrasts, such as T1-weighted image and QSM, may enable more accurate QSM atlas construction[48] or improve brain segmentations in basal ganglia regions.[18] Quantitative MRI measurements, including T1, R2* and QSM from ME-MP2RAGE are similar to those from standard SE-

MP2RAGE and ME-GRE sequences, with a few statistically significant but small differences. However, in general, images produced from ME-MP2RAGE have lower SNR and more blurring than those from standard separate sequences (i.e. SE-MP2RAGE and ME-GRE), mainly due to shorter echo times and longer readout during inversion recovery. Nevertheless, our measured T1 values of brain tissue are in excellent agreement with a previous report at 7 T.[45] R2* and susceptibilities of brain tissue reported in our study are also consistent with 7 T literature.[46,49]

Since the introduction of the original MP2RAGE sequence,[2] numerous variants of the sequence have been proposed, such as monopolar ME-MP2RAGE, which enables T2* and susceptibility-induced contrasts in addition to T1 contrasts. However, the previously proposed ME-MP2RAGE method[3] required a scan time of about 20 minutes and the coil combination technique employed for phase suffered from significant artifacts. Here we propose two modifications to the ME-MP2RAGE sequence to achieve a clinically feasible scan time (~8.5 min), while producing the same array of MR images. We applied GRAPPA in the first phase-encoding dimension, outside of the inversion loop, and used bipolar GRE readouts, instead of the original implementation with GRAPPA in the second phase-encoding dimension and monopolar readouts, to boost the acquisition efficiency and substantially cut the scan time. We note that another recent study modified the sequence to keep a single echo at the first inversion time, while enabling multiple echoes at the second.[5] Shortening scan time is particularly important for studying pediatric and cognitively impaired elderly populations who cannot tolerate long scan durations. In addition to acquisition improvements, we modified ME-MP2RAGE reconstruction pipelines to take advantage of the multiple echoes. It has been shown that multi-echo MP2RAGE achieves higher SNR efficiency over single-echo at 3 T.[4] In this paper, T1-weighted images and T1 maps derived from individual echoes were combined to increase the SNR while maintaining contrast map accuracy.

In the original single-echo[2] and multi-echo[3] MP2RAGE papers, a low flip angle approach was used to minimize the B_1+ inhomogeneity effect. We investigated the effects of using higher flip angles (i.e. 8 and 10 degrees) in our short acquisitions with high sampling bandwidths. A comparison of different flip angles is demonstrated in Supporting Information Figure S7. We observed that: (i) there is less signal dropout in the cerebellum with higher flip angles; (ii) R2* maps calculated from the lower flip angles acquisition are noisier, especially in cerebellum; and (iii) the SNR boost from higher flip angles is less obvious in QSM, which may due to the image

regularization used during dipole inversion. Based on these observations, we adopted the higher flip angles of 8 and 10 degrees. The different results shown in Supporting Information Figure S7 due to different flip angles also suggest the residual B1+ inhomogeneity effects. This B1+ dependency can be further reduced by acquiring an additional B1 map to correct the T1-weighted images and T1 maps according to lookup tables with sequence parameters.[50] Nevertheless, our GRE TR from the proposed ME-MP2RAGE is shorter than the original SE-MP2RAGE, which also leads to lower B1+ contamination.

QSM is a post-processing technique that performs dipole field inversion on local phase[10,40,51–53] or total phase maps[14,54,55] to map the magnetic susceptibility source distribution. Unlike other quantitative MRI metrics, such as T1, T2, and T2*, magnetic susceptibility is a tissue property that is, in theory, independent of magnetic field strength and sequence parameters. A standard multi-echo gradient-echo (ME-GRE) sequence is the most used technique for QSM, while other acquisition methods such as EPI,[55,56] fMRI,[57] or water saturation shift techniques[58] have also been proposed. Phase pre-processing is critical for successful QSM reconstruction. As shown in the previous ME-MP2RAGE paper[3] and also demonstrated in the current study, QSM processed from standard scanner output images can result in substantial artifacts due to phase singularities in the default adaptive combined phase from multiple receiver channels, at ultra-high field with no body coil. Here we have proposed a new technique, called POEM, to estimate and remove the channel-dependent phase-offsets from individual channels before combining them. The POEM method also removes the phase-offset between odd and even echoes from two readout polarities due to eddy currents from the gradients system.[31,33] This enables successful QSM using a more efficient bipolar acquisition. POEM is demonstrated to properly combine phase images from multiple channels without introducing phase singularities, in both ME-MP2RAGE and ME-GRE sequences with bipolar acquisitions. The POEM method does not require a separate reference scan,[27] which can be problematic if the subject's head has moved between calibration and actual scans. It also does not require specific echo times,[28] which significantly constrains the sequence parameters. Compared to other coil combination methods,[59,60] the POEM method completely removes the phase offsets that originate from individual receiver coils and different readout polarities. Robust QSM images with no phase-singularity or bipolar-readout induced artifacts are derived for both ME-MP2RAGE and ME-GRE acquisitions.

The echo times of our ME-MP2RAGE are shorter than those from the Metere et al.'s,[3] due to the fact that we implemented GRAPPA in the first phase-encoding dimension, rather than the second phase-encoding dimension, to achieve a clinically feasible scan time. Even though our echo times are shorter than the optimal values for QSM and R2* at 7 T,[61] no substantial difference is observed in R2* or QSM, comparing our implementation (last TE of 9.10 ms) with Metere's (last TE of 15.82 ms) in Supporting Information Figure S8, except improved SNR in R2* map in the longer scan, especially in cerebellum. This SNR improvement is not apparent in QSM results, likely due to the image regularization process during the dipole inversion. Note that long TEs for the ME-MP2RAGE sequence also come with disadvantages compared to its single-echo version. For example, an increase of TE alters the inversion recovery curve and increases the T1 modulation and blurring effect, which may degrade image quality. Nevertheless, our TEs are relatively short and thus the readout duration is slightly shorter than the Metere implementation, which in theory reduces the T1 blurring. There is also more T2* weighting in the magnitude images from later echoes, which gives a mixed T1-weighted and T2*-weighted contrast in the magnitude image. This may not be ideal for image registration using conventional T1-weighted templates. To extract purer T1-weighted contrast, images from the shortest echo time (TE_1) should be used. Alternatively, one can also acquire single echo in first TI and multiple echoes in second TI, as demonstrated by Caan et al.[5] On the contrary, other studies have been proposed to make use of the mixed T1/T2* contrast to enhance deep grey matter contrast on conventional T1-weighted images to improve basal ganglia segmentation,[62] especially for the globus pallidus.[18]

R2* values estimated from our proposed ME-MP2RAGE in GM regions are in good agreement with the long echo ME-GRE sequence (last echo time of 21.42 ms), while R2* values in WM derived from the ME-MP2RAGE sequence are higher than ME-GRE sequence, and the bias is likely due to the different ranges of echo times. Nevertheless, in the future we will implement parallel imaging techniques, such as GRAPPA or CAIPIRINHA[63] inside the inversion loop to enable longer echo times and shorter readout length, while still maintaining acceptable scan times. This may also eliminate the need for partial Fourier in both phase-encoding directions and thus recover the native spatial resolution from about 1 mm to 0.75 mm isotropic. Current implementation of the ME-MP2RAGE sequence for extracting multi-parametric maps are directly applicable to 7 T only. Increased echo times could also make the

sequence feasible for QSM and SWI at 3 T. The shortened readout length during inversion recovery would also reduce the T1 blurring effect.

CONCLUSIONS

We have presented a bipolar multi-echo MP2RAGE sequence with a scan time of 8 and a half minutes that can produce whole-head, high-resolution, multi-parametric maps simultaneously, including T1-weighted images, T1 map, R2* map, SWI, mIP, and QSM. A reconstruction algorithm is also presented that exploits the multi-echo acquisition to improve SNR and combine the multi-channel phase images in a robust manner. This single ME-MP2RAGE sequence can replace the acquisition of separate MP2RAGE and ME-GRE measurements at 7 T, with the benefits of intrinsic registration of different MRI contrasts and substantially shortened total scan time.

ACKNOWLEDGEMENTS

The authors would like to thank Kieran O'Brien, Tobias Kober, and Siemens Healthcare for technical assistance and access to the works-in-progress MRI sequences. We also thank Multi-modal Australian ScienceS Imaging and Visualisation Environment (MASSIVE) for high-performance computing support. This work was supported by grants from Alberta Innovates Health Solutions (AIHS); Canadian Institutes of Health Research (CIHR) (FDN-143290); Campus Alberta Innovates Program (CAIP); Australian National Imaging Facility (NIF) funded by National Collaborative Research Infrastructure Strategy (NCRIS); University of Melbourne McKenzie Fellowship; NHMRC Peter Doherty Fellowship; RHISE HBI-Melbourne Trainee Research Exchange Program.

REFERENCES

1. Mugler JP, Brookeman JR. Three-dimensional magnetization-prepared rapid gradient-echo imaging (3D MP RAGE). *Magn Reson Med*. 1990;15(1):152-157. doi:10.1002/mrm.1910150117

2. Marques JP, Kober T, Krueger G, van der Zwaag W, Van de Moortele PF, Gruetter R. MP2RAGE, a self bias-field corrected sequence for improved segmentation and T1-mapping at high field. *Neuroimage*. 2010;49(2):1271-1281. doi:10.1016/j.neuroimage.2009.10.002
3. Metere R, Kober T, Möller HE, Schäfer A. Simultaneous Quantitative MRI Mapping of T1, T2* and Magnetic Susceptibility with Multi-Echo MP2RAGE. Grolmusz V, ed. *PLoS One*. 2017;12(1):e0169265. doi:10.1371/journal.pone.0169265
4. Jutras J-D, Wachowicz K, Gilbert G, De Zanche N. SNR efficiency of combined bipolar gradient echoes: Comparison of three-dimensional FLASH, MPRAGE, and multiparameter mapping with VFA-FLASH and MP2RAGE. *Magn Reson Med*. 2017;77(6):2186-2202. doi:10.1002/mrm.26306
5. Caan MWA, Bazin P, Marques JP, Hollander G, Dumoulin SO, Zwaag W. MP2RAGEME: T 1 , T 2 * , and QSM mapping in one sequence at 7 tesla. *Hum Brain Mapp*. 2019;40(6):1786-1798. doi:10.1002/hbm.24490
6. Rauscher A, Sedlacik J, Barth M, Mentzel H-J, Reichenbach JR. Magnetic susceptibility-weighted MR phase imaging of the human brain. *AJNR Am J Neuroradiol*. 2005;26(4):736-742. doi:26/4/736 [pii]
7. Wei H, Cao P, Bischof A, Henry RG, Larson PEZ, Liu C. MRI gradient-echo phase contrast of the brain at ultra-short TE with off-resonance saturation. *Neuroimage*. 2018;175:1-11. doi:10.1016/j.neuroimage.2018.03.066
8. Haacke EM, Xu Y, Cheng Y-CN, Reichenbach JR. Susceptibility weighted imaging (SWI). *Magn Reson Med*. 2004;52(3):612-618. doi:10.1002/mrm.20198
9. de Rochefort L, Liu T, Kressler B, et al. Quantitative susceptibility map reconstruction from MR phase data using bayesian regularization: validation and application to brain imaging. *Magn Reson Med*. 2010;63(1):194-206. doi:10.1002/mrm.22187
10. Schweser F, Deistung A, Lehr BW, Reichenbach JR. Quantitative imaging of intrinsic magnetic tissue properties using MRI signal phase: an approach to in vivo brain iron metabolism? *Neuroimage*. 2011;54(4):2789-2807. doi:10.1016/j.neuroimage.2010.10.070
11. Shmueli K, de Zwart JA, van Gelderen P, Li T-Q, Dodd SJ, Duyn JH. Magnetic susceptibility mapping of brain tissue in vivo using MRI phase data. *Magn Reson Med*. 2009;62(6):1510-1522. doi:10.1002/mrm.22135

12. Liu T, Spincemaille P, de Rochefort L, Kressler B, Wang Y. Calculation of susceptibility through multiple orientation sampling (COSMOS): a method for conditioning the inverse problem from measured magnetic field map to susceptibility source image in MRI. *Magn Reson Med*. 2009;61(1):196-204. doi:10.1002/mrm.21828
13. Wharton S, Bowtell R. Whole-brain susceptibility mapping at high field: a comparison of multiple- and single-orientation methods. *Neuroimage*. 2010;53(2):515-525. doi:10.1016/j.neuroimage.2010.06.070
14. Sun H, Ma Y, MacDonald ME, Pike GB. Whole head quantitative susceptibility mapping using a least-norm direct dipole inversion method. *Neuroimage*. 2018;179:166-175. doi:10.1016/j.neuroimage.2018.06.036
15. Sun H, Walsh AJAJ, Lebel RMM, et al. Validation of quantitative susceptibility mapping with Perls' iron staining for subcortical gray matter. *Neuroimage*. 2015;105:486-492. doi:10.1016/j.neuroimage.2014.11.010
16. Haacke EM, Cheng NYC, House MJ, et al. Imaging iron stores in the brain using magnetic resonance imaging. *Magn Reson Imaging*. 2005;23(1):1-25. doi:10.1016/j.mri.2004.10.001
17. Bilgic B, Pfefferbaum A, Rohlfing T, Sullivan E V., Adalsteinsson E. MRI estimates of brain iron concentration in normal aging using quantitative susceptibility mapping. *Neuroimage*. 2012;59(3):2625-2635. doi:10.1016/j.neuroimage.2011.08.077
18. Cobzas D, Sun H, Walsh AJ, Lebel RM, Blevins G, Wilman AH. Subcortical gray matter segmentation and voxel-based analysis using transverse relaxation and quantitative susceptibility mapping with application to multiple sclerosis. *J Magn Reson Imaging*. 2015;42(6):n/a-n/a. doi:10.1002/jmri.24951
19. Wang Y, Spincemaille P, Liu Z, et al. Clinical quantitative susceptibility mapping (QSM): Biometal imaging and its emerging roles in patient care. *Journal of Magnetic Resonance Imaging*. 2017:1-21.
20. Chen W, Zhu W, Kovanlikaya I, et al. Intracranial calcifications and hemorrhages: characterization with quantitative susceptibility mapping. *Radiology*. 2014;270(2):496-505. doi:10.1148/radiol.13122640
21. Sun H, Kate M, Gioia LC, Emery DJ, Butcher K, Wilman AH. Quantitative susceptibility mapping using a superposed dipole inversion method: Application to intracranial

hemorrhage. *Magn Reson Med*. 2016;76(3):781-791. doi:10.1002/mrm.25919

22. Liu S, Mok K, Neelavalli J, et al. Improved MR venography using quantitative susceptibility-weighted imaging. *J Magn Reson Imaging*. 2014;40(3):698-708. doi:10.1002/jmri.24413
23. Wei H, Dibb R, Zhou Y, et al. Streaking artifact reduction for quantitative susceptibility mapping of sources with large dynamic range. *NMR Biomed*. 2015;28(10):1294-1303. doi:10.1002/nbm.3383
24. Sun H, Klahr AC, Kate M, et al. Quantitative Susceptibility Mapping for Following Intracranial Hemorrhage. *Radiology*. 2018;288(3):830-839. doi:10.1148/radiol.2018171918
25. Rudko D a, Solovey I, Gati JS, Kremenchutzky M, Menon RS. Multiple Sclerosis: Improved Identification of Disease-relevant Changes in Gray and White Matter Using Susceptibility-based MR Imaging. *Radiology*. 2014;272(3):132475. doi:10.1148/radiol.14132475
26. Wiggermann V, Hametner S, Hernández-Torres E, et al. Susceptibility-sensitive MRI of multiple sclerosis lesions and the impact of normal-appearing white matter changes. *NMR Biomed*. 2017;30(8). doi:10.1002/nbm.3727
27. Robinson SD, Dymerska B, Bogner W, et al. Combining phase images from array coils using a short echo time reference scan (COMPOSER). *Magn Reson Med*. 2017. doi:10.1002/mrm.26093
28. Eckstein K, Dymerska B, Bachrata B, et al. Computationally Efficient Combination of Multi-channel Phase Data From Multi-echo Acquisitions (ASPIRE). *Magn Reson Med*. 2018. doi:10.1002/mrm.26963
29. Lebel RM, Eissa A, Seres P, Blevins G, Wilman AH. Quantitative high-field imaging of sub-cortical gray matter in multiple sclerosis. *Mult Scler*. 2012;18(4):433-441. doi:10.1177/1352458511428464
30. Fischl B. FreeSurfer. *Neuroimage*. 2012;62(2):774-781. doi:10.1016/j.neuroimage.2012.01.021
31. Feng W, Neelavalli J, Haacke EM. Catalytic multiecho phase unwrapping scheme (CAMPUS) in multiecho gradient echo imaging: removing phase wraps on a voxel-by-voxel basis. *Magn Reson Med*. 2013;70(1):117-126. doi:10.1002/mrm.24457

32. Walsh DO, Gmitro AF, Marcellin MW. Adaptive reconstruction of phased array MR imagery. *Magn Reson Med*. 2000;43(5):682-690. doi:10.1002/(SICI)1522-2594(200005)43:5<682::AID-MRM10>3.0.CO;2-G
33. Sun H, MacDonald ME, Pike GB. Phase Correction of a Bipolar Gradient-Echo Acquisition for Quantitative Susceptibility Mapping. In: *Int. Soc. Magn. Res. Med. Scientific Meeting*. Singapore; 2016:2987.
34. Sun H, Cleary JO, Glarin R, et al. Multi-channel phase combination for quantitative susceptibility mapping at 7T using Phase-Offsets Estimation from Multi-echoes (POEM) method. In: *Int. Soc. Magn. Res. Med. Scientific Meeting*. Paris; 2018:4993.
35. Robinson S, Grabner G, Witoszynskyj S, Trattnig S. Combining phase images from multi-channel RF coils using 3D phase offset maps derived from a dual-echo scan. *Magn Reson Med*. 2011;65(6):1638-1648. doi:10.1002/mrm.22753
36. Abdul-Rahman HS, Gdeisat M a, Burton DR, Lalor MJ, Lilley F, Moore CJ. Fast and robust three-dimensional best path phase unwrapping algorithm. *Appl Opt*. 2007;46(26):6623-6635. doi:10.1364/AO.46.006623
37. Denk C, Rauscher A. Susceptibility weighted imaging with multiple echoes. *J Magn Reson Imaging*. 2010;31(1):185-191. doi:10.1002/jmri.21995
38. Witoszynskyj S, Rauscher A, Reichenbach JR, Barth M. Phase unwrapping of MR images using Phi UN--a fast and robust region growing algorithm. *Med Image Anal*. 2009;13(2):257-268. doi:10.1016/j.media.2008.10.004
39. Smith SM. Fast robust automated brain extraction. *Hum Brain Mapp*. 2002;17(3):143-155. doi:10.1002/hbm.10062
40. Sun H, Wilman AHAH. Background field removal using spherical mean value filtering and Tikhonov regularization. *Magn Reson Med*. 2014;71(3):1151-1157. doi:10.1002/mrm.24765
41. Li W, Wang N, Yu F, et al. A method for estimating and removing streaking artifacts in quantitative susceptibility mapping. *Neuroimage*. 2015;108:111-122. doi:10.1016/j.neuroimage.2014.12.043
42. Reuter M, Rosas HD, Fischl B. Highly accurate inverse consistent registration: A robust approach. *Neuroimage*. 2010. doi:10.1016/j.neuroimage.2010.07.020
43. Avants BB, Tustison NJ, Song G, Cook PA, Klein A, Gee JC. A reproducible evaluation

of ANTs similarity metric performance in brain image registration. *Neuroimage*. 2011;54(3):2033-2044. doi:10.1016/j.neuroimage.2010.09.025

44. Keuken MC, Bazin PL, Crown L, et al. Quantifying inter-individual anatomical variability in the subcortex using 7T structural MRI. *Neuroimage*. 2014;94:40-46. doi:10.1016/j.neuroimage.2014.03.032
45. Rooney WD, Johnson G, Li X, et al. Magnetic field and tissue dependencies of human brain longitudinal 1H2O relaxation in vivo. *Magn Reson Med*. 2007;57(2):308-318. doi:10.1002/mrm.21122
46. Deistung A, Schäfer A, Schweser F, Biedermann U, Turner R, Reichenbach JR. Toward in vivo histology: a comparison of quantitative susceptibility mapping (QSM) with magnitude-, phase-, and R2*-imaging at ultra-high magnetic field strength. *Neuroimage*. 2013;65:299-314. doi:10.1016/j.neuroimage.2012.09.055
47. Stüber C, Morawski M, Schäfer A, et al. Myelin and iron concentration in the human brain: A quantitative study of MRI contrast. *Neuroimage*. 2014;93(P1):95-106. doi:10.1016/j.neuroimage.2014.02.026
48. Lim IAL, Faria A V., Li X, et al. Human brain atlas for automated region of interest selection in quantitative susceptibility mapping: Application to determine iron content in deep gray matter structures. *Neuroimage*. 2013;82:449-469. doi:10.1016/j.neuroimage.2013.05.127
49. Bilgic B, Xie L, Dibb R, et al. Rapid multi-orientation quantitative susceptibility mapping. *Neuroimage*. 2015;125:1131-1141. doi:10.1016/j.neuroimage.2015.08.015
50. Marques JP, Gruetter R. New Developments and Applications of the MP2RAGE Sequence - Focusing the Contrast and High Spatial Resolution R1 Mapping. *PLoS One*. 2013. doi:10.1371/journal.pone.0069294
51. Wu B, Li W, Guidon A, Liu C. Whole brain susceptibility mapping using compressed sensing. *Magn Reson Med*. 2012;67(1):137-147. doi:10.1002/mrm.23000
52. Liu T, Khalidov I, de Rochefort L, et al. A novel background field removal method for MRI using projection onto dipole fields (PDF). *NMR Biomed*. 2011;24(9):1129-1136. doi:10.1002/nbm.1670
53. Zhou D, Liu T, Spincemaille P, Wang Y. Background field removal by solving the Laplacian boundary value problem. *NMR Biomed*. 2014;27(3):312-319.

doi:10.1002/nbm.3064

54. Liu Z, Kee Y, Zhou D, Wang Y, Spincemaille P. Preconditioned total field inversion (TFI) method for quantitative susceptibility mapping. *Magn Reson Med*. 2016;00(January). doi:10.1002/mrm.26331
55. Langkammer C, Bredies K, Poser BA, et al. Fast quantitative susceptibility mapping using 3D EPI and total generalized variation. *Neuroimage*. 2015;111:622-630. doi:10.1016/j.neuroimage.2015.02.041
56. Sun H, Wilman AHAH. Quantitative susceptibility mapping using single-shot echo-planar imaging. *Magn Reson Med*. 2015;73(5):1932-1938. doi:10.1002/mrm.25316
57. Sun H, Seres P, Wilman AHH. Structural and functional quantitative susceptibility mapping from standard fMRI studies. *NMR Biomed*. 2017;30(4):e3619. doi:10.1002/nbm.3619
58. Lim IAL, Li X, Jones CK, Farrell JAD, Vikram DS, van Zijl PCM. Quantitative magnetic susceptibility mapping without phase unwrapping using WASSR. *Neuroimage*. 2014;86:265-279. doi:10.1016/j.neuroimage.2013.09.072
59. Khabipova D, Wiaux Y, Gruetter R, Marques JP. A modulated closed form solution for quantitative susceptibility mapping - A thorough evaluation and comparison to iterative methods based on edge prior knowledge. *Neuroimage*. 2015. doi:10.1016/j.neuroimage.2014.11.038
60. Liu J, Christiansen SD, Drangova M. Single multi-echo GRE acquisition with short and long echo spacing for simultaneous quantitative mapping of fat fraction, B0 inhomogeneity, and susceptibility. *Neuroimage*. 2018;172:703-717. doi:10.1016/j.neuroimage.2018.02.012
61. Peters AM, Brookes MJ, Hoogenraad FG, et al. T2* measurements in human brain at 1.5, 3 and 7 T. *Magn Reson Imaging*. 2007;25(6):748-753. doi:10.1016/j.mri.2007.02.014
62. Feng X, Deistung A, Dwyer MG, et al. An improved FSL-FIRST pipeline for subcortical gray matter segmentation to study abnormal brain anatomy using quantitative susceptibility mapping (QSM). *Magn Reson Imaging*. 2017;39:110-122. doi:10.1016/j.mri.2017.02.002
63. Breuer FA, Blaimer M, Mueller MF, et al. Controlled aliasing in volumetric parallel imaging (2D CAIPIRINHA). *Magn Reson Med*. 2006. doi:10.1002/mrm.20787

TABLE

Table 1: Summery of key parameters, multi-parametric outputs, and scan time of different sequences at 7 T.

Sequence	Resolution	Echo times	Multi-modal	Parallel imaging	Scan time
ME-GRE	0.75 mm iso	5.10 ms – 21.4 ms (9 bipolar echoes)	SWI, T_2* map, QSM	GRAPPA = 2	9:25 mins
SE-MP2RAGE	0.75 mm iso	2.96 ms	T_1w, T_1 map	GRAPPA = 3	8:12 mins
ME-MP2RAGE	0.75 mm iso	2.38 ms – 9.10 ms (4 bipolar echoes)	T_1w, T_1 map, SWI, T_2* map, QSM	GRAPPA = 3	8:27 mins

FIGURE CAPTIONS

Figure 1: Illustration of the bipolar ME-MP2RAGE sequence diagram. The drawn ME-GRE readouts represent the middle step of the inner phase encoding loop, which corresponds to the center line of k-space in the slice dimension.

Figure 2: Magnitude and phase images of multiple echoes at two inversion times from the ME-MP2RAGE sequence are shown on the left. The simultaneously derived T1-weighted, T1 map, R2* map, SWI, mIP and QSM images from this single acquisition are demonstrated on the right.

Figure 3: (a) T1-weighted images derived at different echo times, as well as the echo-combined image using sum-of-squares (SoS). Zoomed-in images of the white box region illustrating tissue contrast and signal-to-noise are shown at the bottom row of (a); (b) Quantitative T1 maps at different echo times as well as the average. Zoomed-in images in the white box region are shown at the bottom row of (b). Images are acquired from a healthy 56-year-old female.

Figure 4: T1 maps, in three orthogonal slices, of the same subject from the ME-MP2RAGE (left column) and the SE-MP2RAGE (right column) acquisitions. Images are acquired from a healthy 26-year-old male.

Figure 5: (a, b) R2* maps from the 9-echo ME-GRE sequence and 4-echo ME-MP2RAGE sequence, in three orthogonal slices. (c, d) Sum of squared errors of prediction (SSE) from the R2* fitting residuals for both sequences. White boxes in (a) and (b) indicate the ROI drawn for standard deviation measurements.

Figure 6: SWI and mIP along with their zoomed-in images from the single last echo and combined multiple echoes are displayed at the top and bottom rows respectively. Images are acquired from a 35-year-old male.

Figure 7: Demonstration of the improved QSM results using the POEM method for coil combination in two axial slices. The vendor default adaptive combination method (a) results in substantial aritfacts (arrows) in the combined phase, local field and QSM images, while the POEM results (b) are artifact free.

Figure 8: Susceptibility maps, in three orthogonal slices, of the same subject from the ME-MP2RAGE (top row) and the ME-GRE (bottom) acquisitions. Images are acquired from a healthy 32-year-old male.

Figure 9: ROI measurements of T1, R2*, and susceptibility in globus pallidus (GP), substantial nigra (SN), red nucleus (RN), putamen (PU), and caudate nucleus (CN), cerebral white matter (WM), and cortical grey matter (GM) are compared between different sequences, using means and standard deviations from the 9 healthy subjects (age: 32.4 ± 5.4, 1 female). Asterisks indicate significant differences (uncorrected, $P < 0.05$).

Supporting Information Figure S1: T1-weighted images from SE-MP2RAGE, as well as from first, last, and combined echo of ME-MP2RAGE. Zoomed-in region of deep grey matter is shown in the bottom row. Red arrows point to the iron-rich globus pallidus. Images are acquired from a healthy 27-year-old male.

Supporting Information Figure S2: Comparison of quantitative T1 maps from the first echo (first column) and the last echo (second column) of the ME-MP2RAGE sequence in three axial slices. Difference maps are shown in the third column by subtracting T1 (TE4) from T1 (TE1); standard deviation maps as shown in the last column are computed voxel-wise from T1 maps calculated from the 4 different TEs; red arrows point to areas with noticeable differences between the two TEs. Two ROIs are drawn: one in a uniform white matter region (white ellipsoid) and another in the frontal brain region close to sinus (black ellipsoid). Measurements of the two ROIs are reported in the table.

Supporting Information Figure S3: R2* maps of the segmented grey matter (top two rows) and white matter (bottom two rows) from (i) ME-GRE sequence using all the 9 echoes (first column); (ii) the same ME-GRE acquisition but using only the first 3 echoes (middle column); (iii) ME-MP2RAGE sequences using all the 4 echoes (last column). Red arrows point to regions appearing different intensities among the three columns.

Supporting Information Figure S4: SWI images, in two axial slices, of the same subject from the ME-MP2RAGE (left column) and the ME-GRE (right column) acquisitions. Images are acquired from a healthy 25-year-old male.

Supporting Information Figure S5: (a) Odd-echo phase-offsets images of 32 individual channels from the bipolar ME-MP2RAGE sequence; (b) Even-echo phase-offsets images from the opposite readout polarity; (c) Phase-offsets difference between different readout polarities due to eddy currents.

Supporting Information Figure S6: (a) raw phase images of 32 individual channels from the ME-GRE sequence; (b) corrected phase after phase-offset removal; (c) local field maps and (d) QSM in orthogonal slices containing basal ganglia.

Supporting Information Figure S7: Coronal T1w, R2* and QSM slices from the ME-MP2RAGE sequence with flip angles of 4/5 and 8/10. Cerebellum is zoomed-in for better visual comparison between different flip angles.

Supporting Information Figure S8: Orthogonal slices of the R2* maps and QSM generated by our proposed 4-echo ME-MP2RAGE sequence and the 7-echo Metere version. Red arrows point to noticeable differences in R2*.

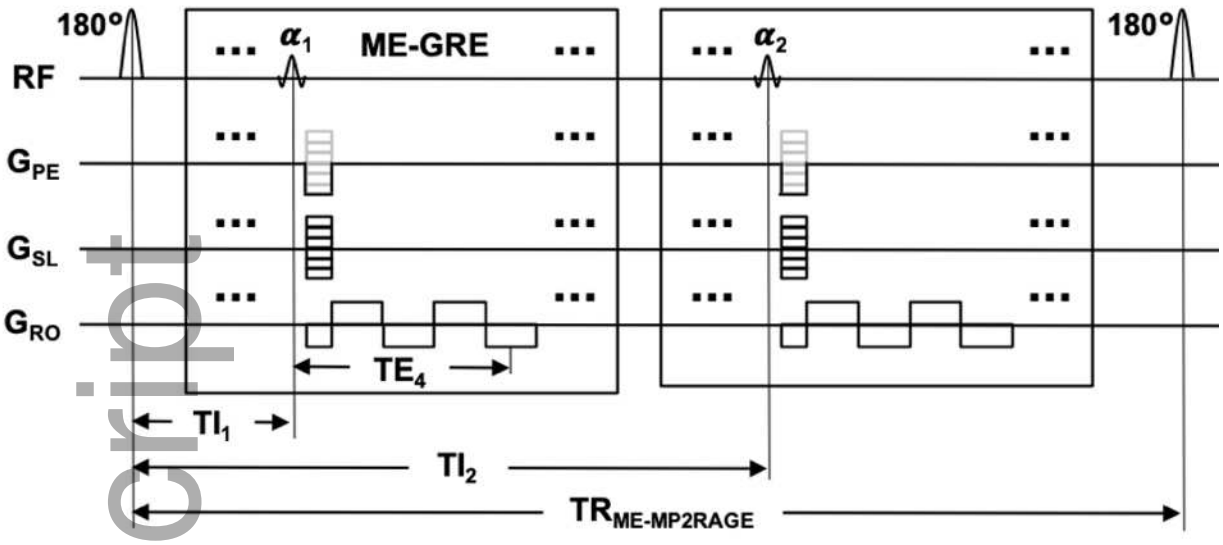

mrm_27975_f1.tif

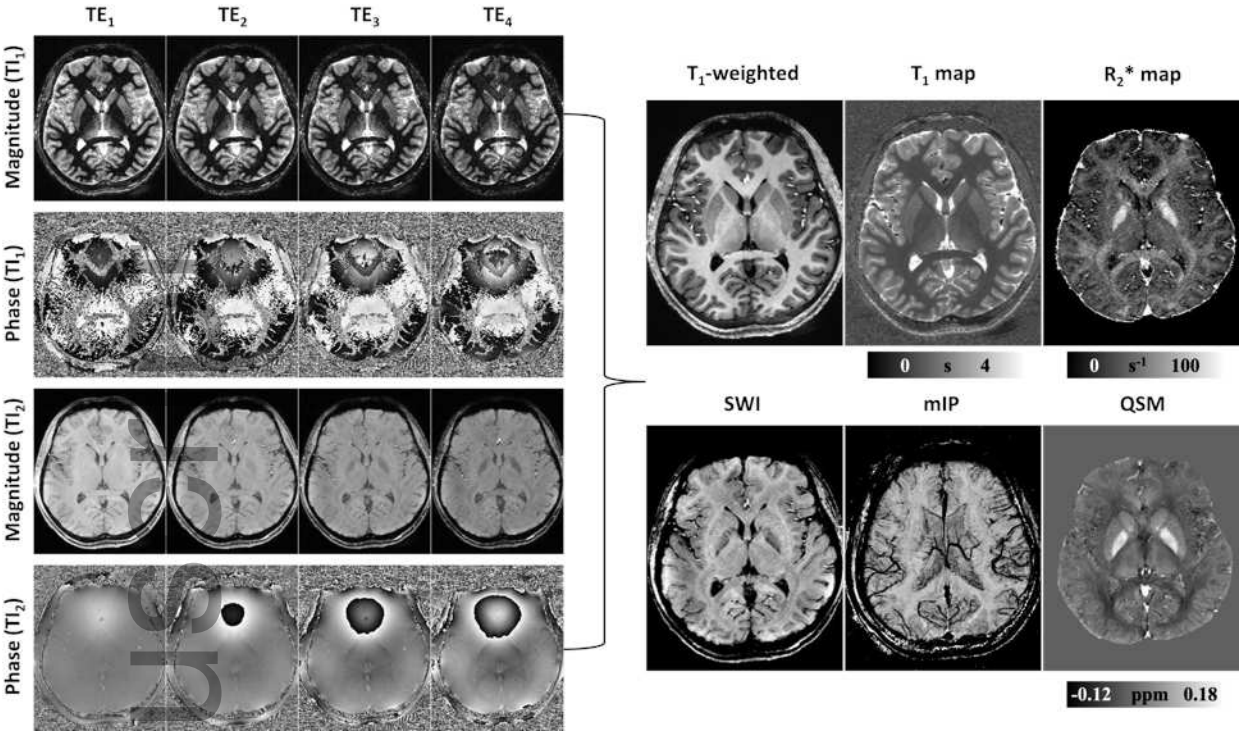

mrm_27975_f2.tif

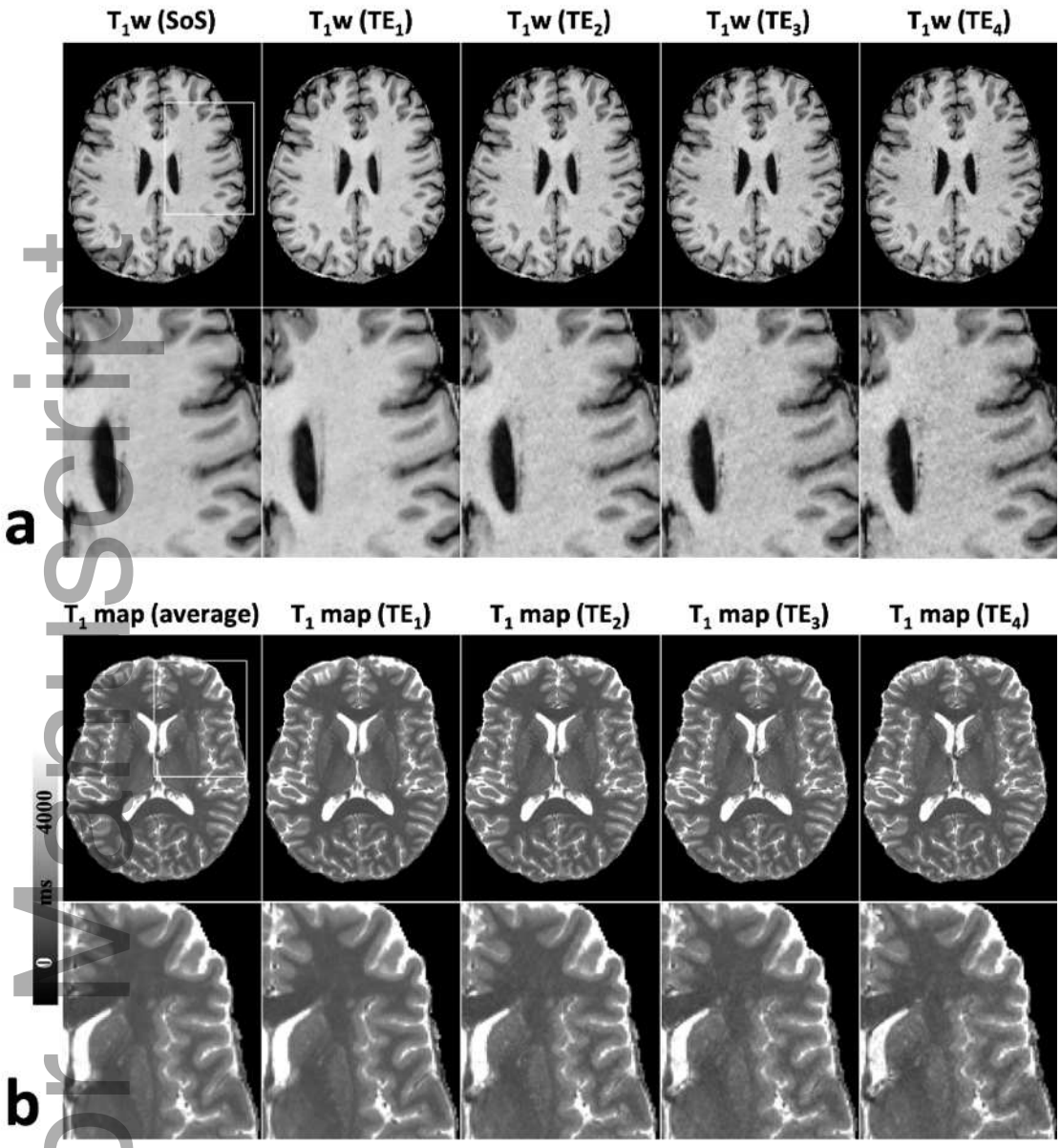

mrm_27975_f3.tif

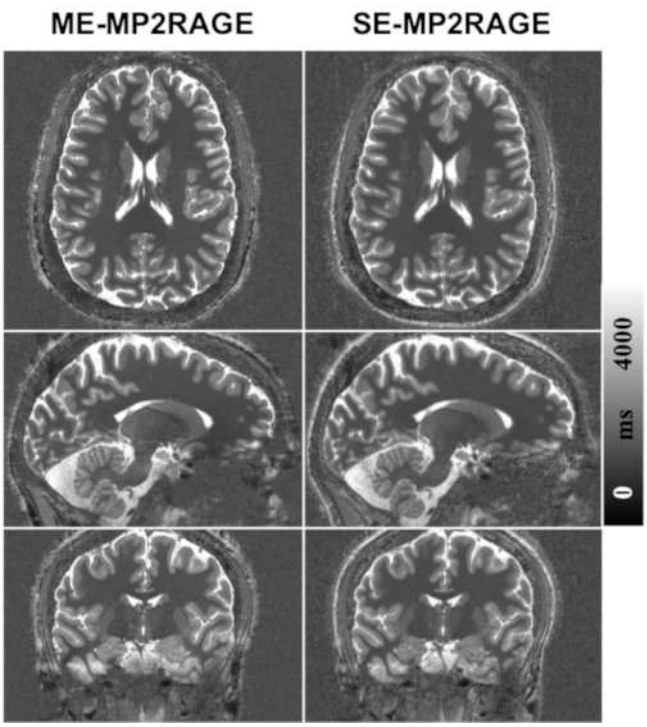

mrm_27975_f4.tif

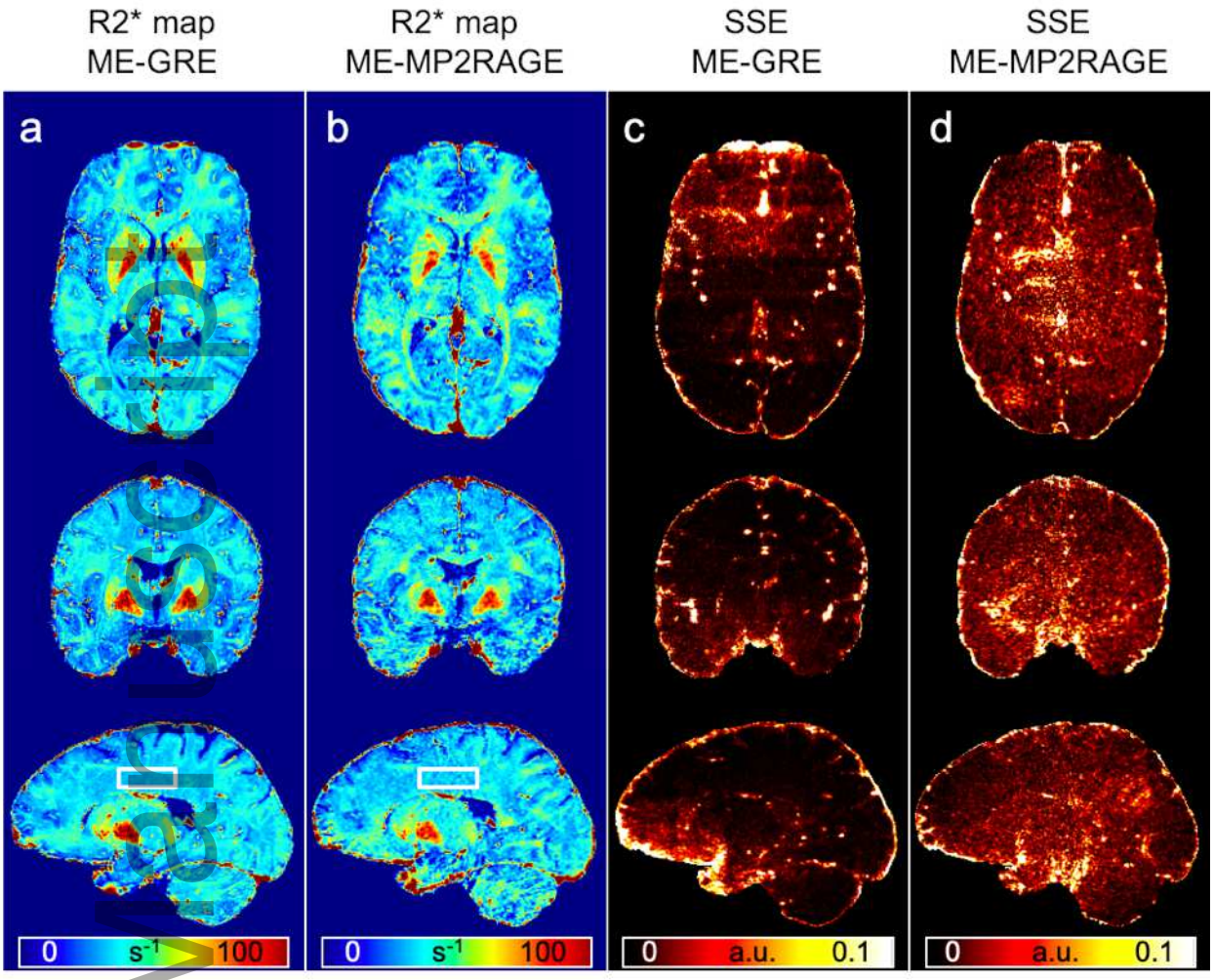

mrm_27975_f5.tif

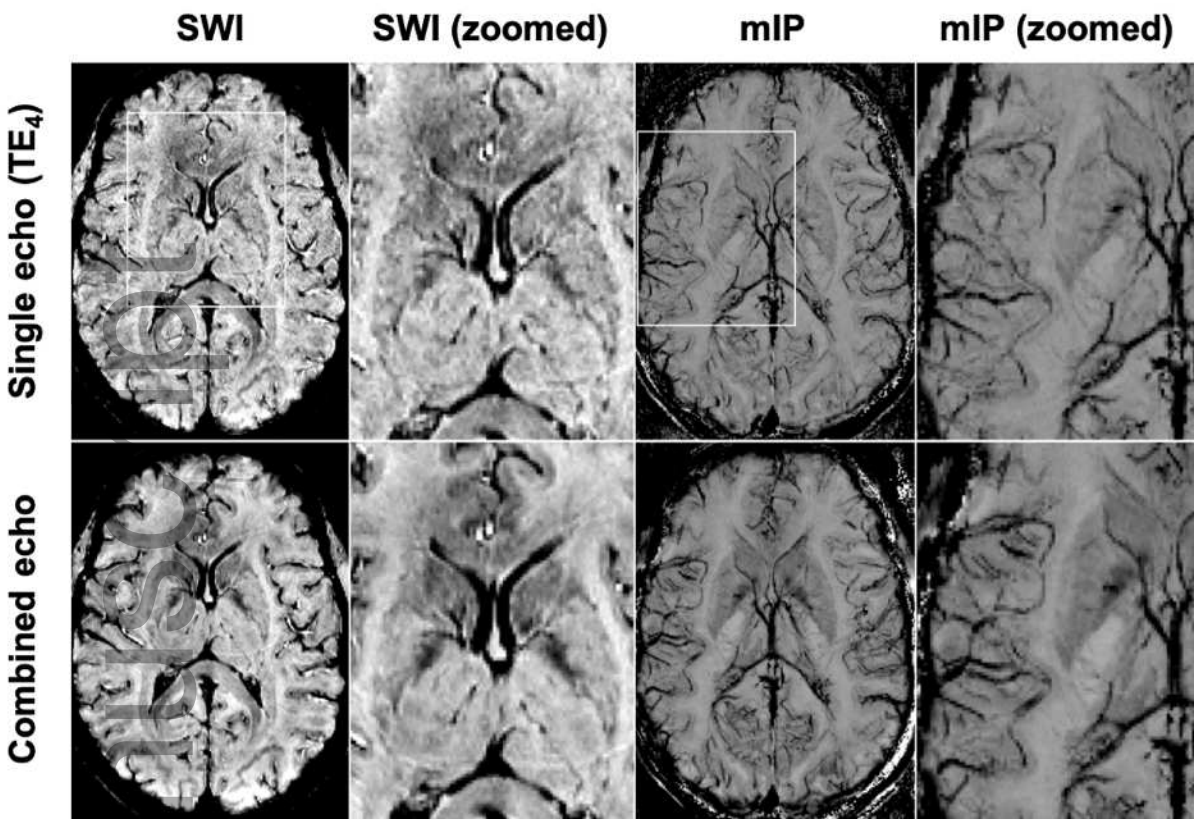

mrm_27975_f6.tif

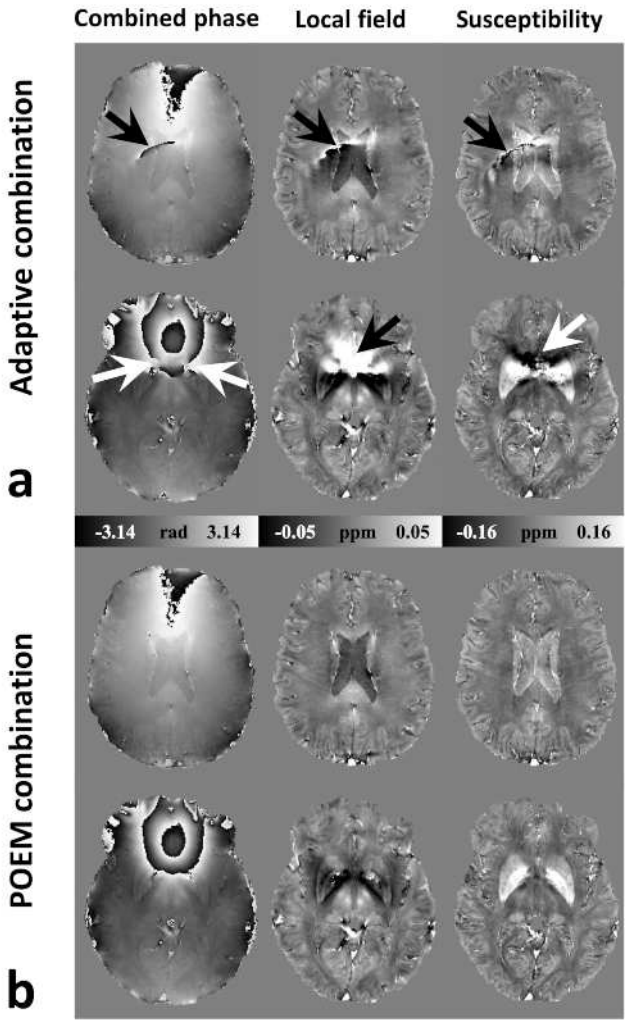

mrm_27975_f7.tif

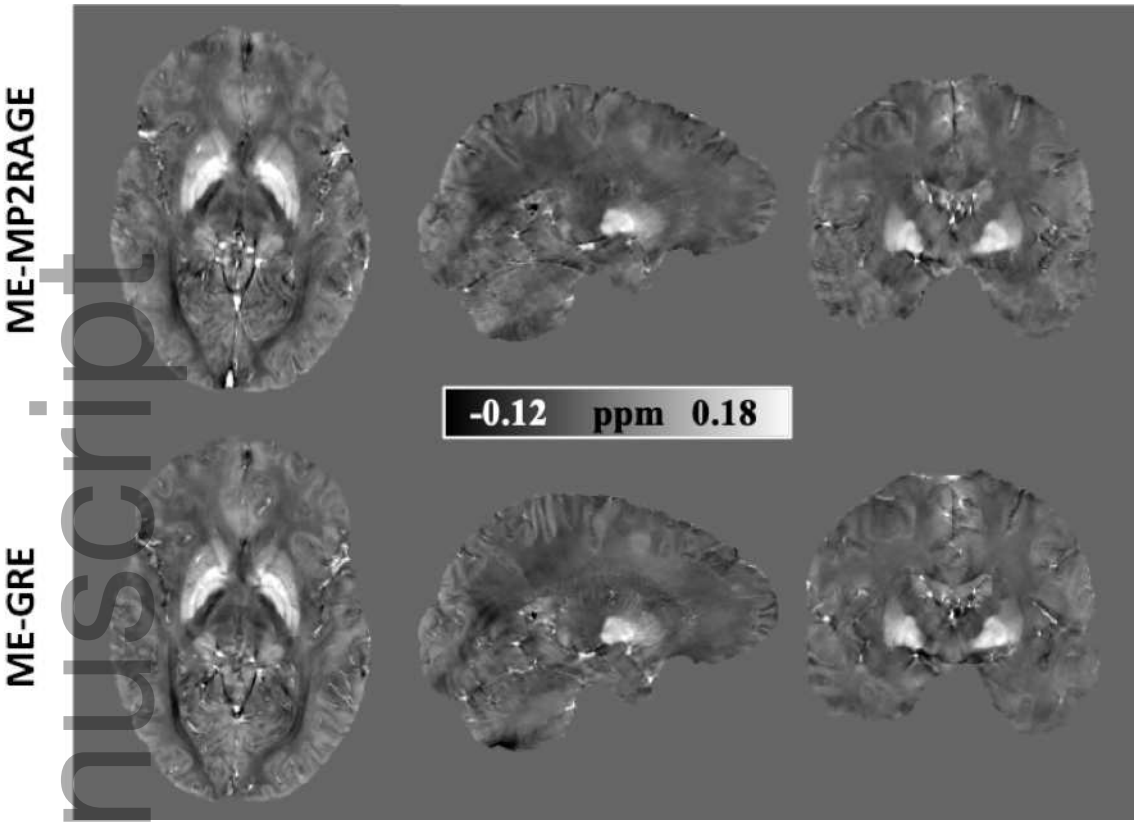

mrm_27975_f8.tif

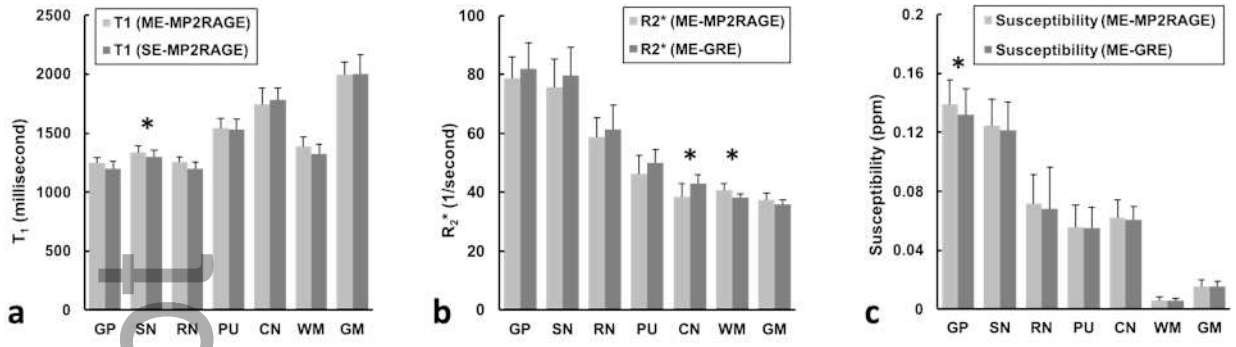

mrm_27975_f9.tif